UNIVERSITY OF CALIFORNIA,
IRVINE

Filter Diagonalization Method as a High Resolution Spectral Estimator

THESIS

submitted in partial satisfaction of the requirements for the degree of

MASTER OF SCIENCE
in Chemistry

by

Jianhan Chen

Committee in Charge:
Professor Vladimir A. Mandelshtam, Chair
Professor David A. Brant
Professor Christopher J. Grayce

2000

The thesis of Jianhan Chen is approved:

_____

_____

_____

Committee Chair

University of California, Irvine

2000

DEDICATION

To my parents, my brothers, and all those who I love

TABLE OF CONTENTS

LIST OF FIGURES

ACKNOWLEDGEMENTS

First, I would like to thank my advisors, Professor Vladimir A. Mandelshtam and Professor A. J. Shaka, for their support, encouragement, and inspiration during the last two years. I thank Prof. Mandelshtam for his patience, and the many long hours he spent talking with me about the research projects. I thank both advisors for being great mentors and for their enthusiasm and determinations in pursuing science.

Special thanks go to Professor Ara Apkarian and Professor Peter Taborek for offering me the great chance to study in Chemical and Materials Physics (ChaMP) program. I am grateful to Professor Ara Apkarian for his enthusiastic support and encouragement. I must also thank Michele W. Tsui for her very kind helps.

I would like to thank Dr. Haitao Hu for his very helpful assistance. Also many thanks to my colleagues Anna A. De Angelis, Joseph Curtis, Mari A. Smith and Nathan D. Taylor. I thank Anna A. De Angelis and I-Feng William Kuo for proof reading this thesis. I am especially indebted to I-Feng William Kuo for making my life, particularly that with computer, much easier.

Finally, I would like to thank the Department of Chemistry at UC-Irvine for giving me the chance to study in USA.

ABSTRACT OF THE THESIS

Filter Diagonalization Method as a High Resolution Spectral Estimator

By

Jianhan Chen

Master of Science in Chemistry

University of California, Irvine, 2000

Professor Vladimir A. Mandelshtam, Chair

The theory of the Filter Diagonalization Method (FDM) for processing NMR signal is briefly reviewed. Stability and performance of FDM for harmonic inversion (i.e. fitting a time signal by $C(t) = \sum_k d_k e^{-it\omega_k}$) of noisy data is examined. Although FDM is capable to extract accurately the parameters of narrow spectral peaks, in the presence of broad peaks (or strong background spectrum) and noise,the FDM *ersatz* spectrum , i.e. $I(\omega) = \sum_k d_k/(\omega_k - \omega)$, maybe distorted in some regions and be sensitive to the FDM parameters, such as window size, window position, etc. Some simple hybrid methods, namely, hybrid FDM+FT, hybrid FT+FDM and hybrid FDM+FDM, that can correct the ersatz spectrum, are discussed. Then, a more consistent approach, the *multi-scale* FDM, is introduced to solve the instability problem, in which some coarse basis vectors describing (in low resolution) the global behavior of the spectrum are added to the narrow band Fourier basis. The *multi-scale* FDM is both stable and accurate, even when the total size of the basis (i.e., the number of coarse plus narrow band basis vectors) used is much smaller than what would previously be considered as necessary for FDM. This, in turn, significantly reduces the computation cost. Extension of the 1D *multi-scale* FDM to a multi-dimensional case is also presented.

General Introduction

The two fundamental problems in NMR spectroscopy, as well as in most other spectroscopies, are resolution and sensitivity. During the last decade, sensitivity has been steadily improved with new advances in NMR probe design and high-field magnet technology. However, the fundamental resolution solely depends on the attainable magnetic field strength and has seen only very limited improvement over the same time frame. Conventional pulsed NMR has been known as Fourier Transform NMR (FT-NMR), because it depends solely on FT to transform the time signals to spectra. The Fourier transform is a linear method that is considered fast, numerically stable and highly reliable. However, in frame of FT, the spectral resolution in each frequency dimension is limited by the so called *FT time-frequency uncertainty principle*,

$$\delta F_l \sim \frac{1}{N_l \tau_l} \ , \tag{1.1}$$

where N_l is the number of acquired time-domain points and τ_l is the sampling time interval. Since each increment in an interferometric dimension requires at least one repetition of the entire pulse sequence, the time signal is almost always truncated in the indirect dimensions, especially in the case of high-dimensionality experiment, leading to poor resolution in these dimensions. In addition, an absorption-mode spectrum is always desired. In the 1D case it is obtained by simply taking the real part of the FT spectrum after it is correctly phased; in 2D NMR purely phase modulated signals give rise to mixed-phase ("phase-twist") line-shapes in which neither the real nor the imaginary part of a 2D FT spectrum can be phased to the desired double-absorption line-shape [14]. Absorption-mode 2D spectra can be obtained from a pair of amplitude-modulated signals or from a pair of N- and P-type data sets by taking appropriate linear combinations [16], which necessitates using data sets twice as large. In 3D NMR the triple-absorption line-shape is obtained by using 2^2 bigger sets. Note though that in some experiments, as in 2D-J, the hyper-complex signals

are unavailable, so that only absolute-value spectra can be obtained, which leads to poor resolution. Due to these problems, extensive efforts have been devoted to the development of alternative techniques to FT. The various methods proposed include linear prediction (LP), maximum entropy reconstruction, maximum likelihood, Bayesian analysis etc [15]. Despite the long history of these alternatives, none of them has been widely used in practical analysis of typical NMR signals. The main reason may be that these methods are computationally expensive, numerically unstable and can lead to unreliable results. Thus, Fourier transform remains the method of choice for NMR data processing.

Recently, the Filter Diagonalization Method (FDM) has emerged as a powerful high-resolution alternative method to FT for processing time signals. FDM possesses some unique features which, in certain respects, makes it superior to the other method. For some 1D problems, especially involving long and noiseless signals, FDM is extremely efficient. However, its actual strength reveals outside the 1D applications. In multi-dimensional FDM, the whole multidimensional data set is processed simultaneously and fit into a certain multidimensional parametric form. The resolution in every dimension is limited by the total number of time signal points, $N_{\text{total}} = N_1 \times N_2 \times \ldots \times N_{\text{D}}$, instead of being limited by the number of signal points in each dimension separately. This makes it possible to use longer running time data acquisition to enhance the resolutions in the indirect dimensions. In addition, FDM can be used to compute various non-trivial reduced-dimensionality projections like absorption mode 45^o projection of a 2D-J spectrum [10]. Compared to other high-resolution methods like Linear Prediction (LP), FDM does not require a good guess of parameters to be used and usually gives reliable results. In the rest of this thesis, the basic theory of FDM will be first introduced in Chapter I, then an improved version of FDM, *Multi-Scale* FDM, introduced in Chapter II.

Chapter I

Theory of the Filter Diagonalization Method (FDM) for NMR Data Processing

1.1 1D FDM

The Filter Diagonalization Method (FDM) was originally designed by Neuhauser [1] for iterative diagonalization of large matrices which arise in quantum dynamics calculations when using a time-dependent approach. Later, it was reformulated [2] and split into two independent steps, namely, generation of a quantum time correlation function and its spectral analysis (*harmonic inversion*). In this new formulation FDM is suitable for spectral analysis of a general experimentally-measured time signal, simply by ignoring the first step of signal generation. At this point, FDM was conceptually new and potentially very promising, but its implementation was numerically inefficient. Mandelshtam and Taylor [3] reformulated it for the conventional problem of processing a time signal defined on an evenly-spaced time grid, and found a way to significantly improve its performance. FDM has since found many applications in diverse fields and in particular for processing NMR time signals [5–12].

The basic object of 1D FDM is to fit a given complex time signal (FID) $c(n) = C(t_n)$, defined on an equidistant time grid $t_n = n\tau, n = 0, 1, 2, \ldots, N-1$, to the sum of exponentially damped sinusoids,

$$c(n) = \sum_{k=1}^{K} d_k e^{-in\tau\omega_k} = \sum_{k=1}^{K} d_k e^{-in2\pi\tau f_k} e^{-n\tau\gamma_k} \tag{1.2}$$

with a total of $2K$ unknowns: the K complex amplitudes d_k and complex frequencies $\omega_k = 2\pi f_k - i\gamma_k$, which include the exponential damping. We call the *line list* $\{\omega_k, d_k\}$ a *parameter representation* of the signal, and every peak specified by a pair of ω_k and d_k a pole. This problem is often referred to as the *Harmonic Inversion Problem* (HIP). Although it is highly nonlinear, its solutions can be obtained by pure linear algebra. We assume that the complex time signal $c(n)$ is associated with a time autocorrelation

function of a fictious dynamical "Hamiltonian" operator $\hat{\Omega}$ with complex eigenvalues $\{\omega_k\}$ [2],

$$c(n) = \left(\Phi_0 \middle| e^{-in\tau\hat{\Omega}}\Phi_0\right) \ . \tag{1.3}$$

Here a complex symmetric inner product is used, $(a|b) = (b|a)$ without complex conjugation. Φ_0 is some arbitrary"initial state" (as will be clear later, neither $\hat{\Omega}$ nor Φ_0 is needed to known explicitly). Assume that there is a set of orthonormal eigenvectors, $\{\Upsilon_k\}$, that diagonalizes $\hat{\Omega}$, then we can write,

$$\hat{\Omega} = \sum_k \omega_k |\Upsilon_k)(\Upsilon_k| \ . \tag{1.4}$$

where the eigenvectors are orthonormalized with respect to the complex symmetric inner product, i.e.,

$$(\Upsilon_k|\Upsilon_{k'}) = \delta_{kk'} \ . \tag{1.5}$$

Inserting Eq. 1.4 into Eq. 1.3, we obtain Eq. 1.2 with

$$d_k^{1/2} = (\Upsilon_k|\Phi_0) \ . \tag{1.6}$$

Therefore the harmonic inversion problem of Eq. 1.2 becomes equivalent to diagonalizing the "Hamiltonian" $\hat{\Omega}$ or, equivalently, the evolution operator $\hat{U} \equiv e^{-i\tau\hat{\Omega}}$:

$$\hat{U}\Upsilon_k = u_k\Upsilon_k \ , \tag{1.7}$$

with $u_k = e^{-i\tau\omega_k}$. The *eigenvalues* of $\hat{U}$ thus determine $\{\omega_k\}$, *line positions* and *widths*, and the *eigenvectors* determines $\{d_k\}$, *line amplitudes* and *phases*.

Even though neither of $\hat{U}$ or Φ_0 is explicitly available, the matrix representation of $\hat{U}$ in an appropriately chosen basis set $\{\Psi_j\}$ can be computed purely from the time signal $c(n)$. The basis, which is not necessarily orthonormal, can be chosen in many different ways. Chosen naïvely, the number of basis functions would determine the size of the linear system which must be solved. For an FID of N complex points, the

maximum basis size is N/2: each Lorentzian line requires two complex numbers to specify it, so that at most $M = N/2$ lines can be uniquely fitted to a signal of length N.

1.1.1 Krylov Basis

The simplest basis would correspond to a set of Krylov vectors $|\Phi_n), n = 0, 1, 2, \ldots, M-1,$ with $M = N/2$, generated by the evolution operator $\hat{U}$:

$$|\Phi_n) = \hat{U}^n|\Phi_0) = \exp(-in\tau\hat{\Omega})|\Phi_0). \tag{1.8}$$

Based on Eq. 1.3, the matrix elements of $\hat{U}$ in this basis are trivial to obtain as

$$U^{(1)}_{nm} = \left(\Phi_n|\hat{U}|\Phi_m\right) = (\Phi_n|\Phi_{m+1}) = c(n+m+1)\ . \tag{1.9}$$

Since the Krylov basis is not orthonormal, the overlap matrix

$$U^{(0)}_{nm} = (\Phi_n|\Phi_m) = c(n+m), \tag{1.10}$$

must also be assembled. Here convenient notations $U^{(1)}$and $U^{(0)}$ are adopted to represent the matrix representations of $\hat{U}$ and overlap matrix. The fitting problem of Eq. 1.2, or equivalently, the operator eigenvalue problem of Eq. 1.4, is then cast into a generalized complex symmetric eigenvalue problem

$$\mathbf{U}^{(1)}\mathbf{B}_k = u_k\mathbf{U}^{(0)}\mathbf{B}_k\ . \tag{1.11}$$

The eigenvalues $u_k = e^{-i\tau\omega_k}$ then yield the frequencies ω_k and the eigenvectors $\mathbf{B}_k$, the amplitudes d_k:

$$d_k^{1/2} = \sum_{n=0}^{M-1}[\mathbf{B}_k]_n\,(\Phi_n|\Phi_0) = \sum_{n=0}^{M-1}[\mathbf{B}_k]_n\,c(n)\ , \tag{1.12}$$

which follows from Eq. 1.6 by substituting

$$|\Upsilon_k) = \sum_{n=0}^{M-1} [\mathbf{B}_k]_n \, |\Phi_n) \ , \tag{1.13}$$

Note that the eigenvectors $\mathbf{B}_k$ are normalized with respect to the overlap matrix $\mathbf{U}^{(0)}$ since the Krylov basis used here is not a orthonormal basis,

$$\mathbf{B}_k^T \mathbf{U}^{(0)} \mathbf{B}_{k'} = \delta_{kk'}. \tag{1.14}$$

Example: model signal with 2 lines.

The simplest nontrivial example of HIP corresponds to the case of two sinusoids ($K = 2$ in Eq. 1.2, i.e., we assume that the signal is

$$c_n = de^{-in\tau(\omega-\Delta\omega)} + d'e^{-in\tau(\omega+\Delta\omega)} \ , \tag{1.15}$$
$$n = 0, 1, 2..., N-1 = 2M-1$$

The case of $M = 1$

Although we know that with just one basis function we cannot possibly get two eigenvalues, we consider this case as it reveals some interesting property of FDM.

$M = 1$ corresponds to the total signal length $N = 2$, i.e., only two signal points will be used. Eq. 1.11 for this case boils down to the 1×1 generalized eigenvalue problem,

$$c_1 \mathbf{B}_1 = u_1 c_0 \mathbf{B}_1 \ .$$

There is only one eigenvalue

$$u_1 \equiv e^{-i\tau\omega_1} = \frac{c_1}{c_0} = e^{-in\tau\omega} \frac{de^{-i\tau\Delta\omega} + d'e^{i\tau\Delta\omega}}{d+d'} \ . \tag{1.16}$$

The eigenvector, which is just a number, after normalized according to Eq. 1.14), $\mathbf{B}_1 c_0 \mathbf{B}_1 = 1$, is given by

$$\mathbf{B}_1 = 1/\sqrt{c_0} \ .$$

Therefore the solution for the amplitude (see Eq. 1.12) is

$$d_1 = \mathbf{B}_1 c_0 = d + d' \ . \tag{1.17}$$

That is, a single-sinusoid-fit of a sum of two complex sinusoids has an amplitude equal to the sum of the two amplitudes and oscillates with a frequency which is some weighted average of the two underlying frequencies. Close inspection of Eq. 1.16 shows that even if both genuine frequencies $\omega \pm \Delta\omega$ were purely real, the solution given by ω_1 will be complex, i.e., will have some width of order of $\Delta\omega$ to account for the two peaks separated by $2\Delta\omega$. In other words, the spectrum given by this single Lorentzian line will be of a low resolution type. Also note, that in the $\Delta\omega \to 0$ limit, i.e. the single sinusoid case, Eq. 1.16 and 1.17 recover the exact result as they should.

The case of $M = 2$

The case of two Krylov basis functions requires the use of $N = 4$ signal points and needs the solution of the following 2×2 generalized eigenvalue problem,

$$\begin{pmatrix} c_1 & c_2 \\ c_2 & c_3 \end{pmatrix} \begin{pmatrix} [\mathbf{B}_k]_1 \\ [\mathbf{B}_k]_2 \end{pmatrix} = u_k \begin{pmatrix} c_0 & c_1 \\ c_1 & c_2 \end{pmatrix} \begin{pmatrix} [\mathbf{B}_k]_1 \\ [\mathbf{B}_k]_2 \end{pmatrix}$$

The eigenvalues can be found from the roots of the characteristic quadratic polynomial,

$$\det \begin{pmatrix} c_1 - u_k c_0 & c_2 - u_k c_1 \\ c_2 - u_k c_1 & c_3 - u_k c_2 \end{pmatrix} = 0 \ .$$

Substitute the assumed form for c_n's (Eq. 1.15), one can check that the two roots are $e^{-in\tau(\omega \pm \Delta\omega)}$. Solving for the eigenvectors, normalizing them according to Eq. 1.14, and using Eq. 1.12 then recovers the two amplitudes, $d_1 = d$ and $d_2 = d'$.

Therefore, for a noiseless signal made of two complex sinusoids the spectral parameters can be calculated to machine accuracy using just four signal points, no matter how close the two frequencies are to each other. This is quite different from

the conventional FT spectral analysis which will require a very fine frequency grid (with the spacing less than $\Delta\omega$) and therefore many time-domain points to resolve two very close lines, no matter how high the signal to noise ratio (SNR) is. That is, the FT cannot take the full advantage of the high SNR, while in parametric fit of the signal the sensitivity is naturally converted into high resolution. It might also be useful to notice that for $M > K$ (here $K = 2$) the $\mathbf{U}^{(1)}$ and $\mathbf{U}^{(0)}$ matrices will indeed be singular with $M - K$ zero eigenvalues. In such a case, solving the generalized eigenvalue problem Eq. 1.11 requires special algorithms such as the QZ-algorithm [17] which can take care of the singularities. It can be checked that for, e.g., $M = 3$ the corresponding 3×3 generalized eigenvalue problem will have the same $K = 2$ correct eigenvalues, and the two eigenvectors will result in the correct amplitudes.

Armed with Eq. 1.9, Eq. 1.10 and Eq. 1.11, the problem is certainly easy to set up, but it is unfortunately very difficult to solve. The $\mathbf{U}$ matrices are dense and far from diagonal. Furthermore, a typical 1D NMR signal will contain several thousands data points, which will lead to matrices with dimension of about a few thousand by a few thousand. A typical eigenvalue solver numerically scales as M^3. Thus, huge matrices are very unfavorable. In addition, if the signal happens to contain far less than M peaks ($K \ll M$), then the basis will be over-complete and the matrices will by ill-conditioned or singular (in case of no noise). The result of these practical considerations is that, formulated in this way, the fitting problem, is a huge and ill-conditioned linear system. This means that it cannot be applied on a regular basis to signals of size more than, say, a few thousand data points. Fortunately, the problem is not so bad as it seem. There is a way to avoid diagonalizing the huge matrices in one step by applying a special unitary transformation to the data matrices $\mathbf{U}^{(1)}$ and $\mathbf{U}^{(0)}$ to make them suitable for a small subspace diagonalization, which is to be introduced in the next section.

1.1.2 Fourier Basis

The primitive Krylov basis functions are not the only choice. Any linear combination of them will serve as a basis. Among them, a good choice would be a Fourier transform of the Krylov basis, of which a particularly simple and efficient variant is the rectangular window Fourier basis [3], defined as

$$|\Psi_j) = \sum_{n=0}^{M-1} e^{in\varphi_j} |\Phi_n) \ , \tag{1.18}$$

with $\{\varphi_j\}$ being a set of equidistant values taken inside a small frequency window of interest. For this choice the transformation from the Krylov basis $\{\Phi_n\}$, $n = 0, 1, 2, ..., M-1$, to the Fourier basis $\{\Psi_j\}$, $j = 1, 2, ..., M$, is unitary. More importantly, due to the Fourier transform, each basis function $|\Psi_j)$ is localized in the frequency domain, i.e., it is a linear combination of only those eigenfunctions $|\Upsilon_k)$ of $\hat{\Omega}$ for which $\omega_k \sim \varphi_j$. This implies that we can consider a small subset of, say, $K_{\rm win} \ll M$ values φ_j in the frequency region $[\omega_{\rm min}, \omega_{\rm max}]$ where *

$$|\Upsilon_k) = \sum_{\omega_k \sim \varphi_j} \left[\tilde{\mathbf{B}}_k\right]_j \Phi_j \ . \tag{1.19}$$

This means that the operator $\hat{U}$ can be diagonalized in the Fourier subspace corresponding to some pre-specified frequency window to yield the eigenvalues and eigenvectors from this window. By choosing another window one can obtain another subset of converged eigenvalues and eigenvectors, and so on. Note that the extraction of the eigenfrequencies ω_k to a high precision only requires that the local completeness condition,

---

*A tilde($\sim$) is added to notation $\mathbf{B}$ because $|\Upsilon_k)$ is now expanded in a different basis other than Krylov basis. It will also be added notation $\mathbf{U}$, the matrix representation of $\hat{U}$ operator in the FT basis.

$$\rho(\varphi_j) = \frac{M\tau}{2\pi} \geq \rho(\omega_k) \ , \tag{1.20}$$

be satisfied for the densities of the grid points $\rho(\varphi_j)$ and that of the eigenfrequencies $\rho(\omega_k)$. In other words, the number $K_{\rm win}$ of the basis vectors Φ_j should be larger than the number of the eigenvalues in the small interval $[\omega_{\rm min}, \omega_{\rm max}]$. Moreover, the local spectral analysis not only avoids problems of estimating the total rank K of the signal subspace, but to certain extent it is also insensitive to the spectral properties outside the chosen small spectral domain.

The matrix elements of the evolution operator $\hat{U}^{(p)} \equiv e^{-ip\tau\hat{\Omega}}$ between any two Fourier basis functions $|\Psi_j)$ and $|\Psi_{j'})$, defined by Eq. 1.18, can also be evaluated only in terms of the measured signal $c(n)$. Let us define the matrix elements of $\hat{U}^{(p)}$ in the Fourier basis

$$\left[\tilde{\mathbf{U}}^{(p)}\right]_{jj'} = \left(\Psi_j|\hat{U}^{(p)}\Psi_{j'}\right) . \tag{1.21}$$

Since the vectors $|\Psi_j)$ defined by Eq. 1.18 are linear combinations of the primitive Krylov vectors $|\Phi_n)$, the matrix elements of $\hat{U}^{(p)}$ in the Fourier basis are also functions of only the $\{c(n)\}$ sequence and do not depend explicitly on either of the auxiliary objects $\hat{U}$, $|\Upsilon_k)$ or $|\Phi_0)$. Inserting Eq. 1.18 into Eq. 1.21 and using the result of Eq. 1.9, we have

$$\left[\tilde{\mathbf{U}}^{(p)}\right]_{jj'} = \sum_{n'=0}^{M-1}\sum_{n=0}^{M-1} e^{in\varphi_j} e^{in'\varphi_{j'}} c(n+n'+p) \ . \tag{1.22}$$

This double sum can be simplified to a single sum by changing the variables from (n, n') to $(l = n+n', n')$ and then summing over n', which, after some algebra, gives:

$$\begin{aligned}\left[\tilde{\mathbf{U}}^{(p)}\right]_{jj'} &= \hat{S}\sum_{\sigma=0,1}\frac{e^{i\sigma[\tau M(\varphi_{j'}-\varphi_j)+\pi]}}{1-e^{i\tau(\varphi_{j'}-\varphi_j)}} \\ &\times \sum_{n=\sigma M}^{(\sigma+1)(M-1)} e^{in\tau\varphi_j} c(n+p) \ ,\end{aligned} \tag{1.23}$$

where $\hat{S}$ defines symmetrization operator over the indices j and j':

$$\hat{S}\ g_{jj'} = g_{jj'} + g_{j'j}\ . \tag{1.24}$$

Eq. 1.23 is, in principle, correct for all choices of φ and $\varphi_{j'}$ except for the singularity arising at $\varphi_j = \varphi_{j'}$. To obtain a numerically practical expression for this singular case we evaluate the $\varphi_j \to \varphi_{j'}$ limit leading to

$$\left[\tilde{\mathbf{U}}^{(p)}\right]_{jj} = \sum_{n=0}^{2M-2} e^{in\tau\varphi_j}(M - |M-n-1|)c(n+p)\ . \tag{1.25}$$

Notably and quite importantly, the resulting matrices $\tilde{\mathbf{U}}^{(p)}$ have a sinc-like structure with generally large diagonal and decaying off-diagonal terms as expected. The latter become much smaller than the former once $M\tau|\varphi_j - \varphi_{j'}| \gg 2\pi$. It is this structure which justifies the possibility to perform the eigenvalue calculation in a small $K_{\text{win}} \times K_{\text{win}}$ block fashion for possibly large $M \times M$ matrices $\tilde{\mathbf{U}}^{(p)}$. In another word, now we can analyze the whole spectrum, which could be complicated and contain thousands of peaks, by breaking it into small pieces.

After the new matrix representations are computed, one can plug them into the same generalized complex eigenvalue equation (Eq. 1.11) and solve for eigenvalue $\{u_k\}$ and eigenvectors $\tilde{\mathbf{B}}_k$. According to Eqs. 1.6 and 1.18 the amplitudes d_k can be easily computed using

$$d_k^{1/2} = \tilde{\mathbf{B}}_k^{\mathrm{T}}\tilde{\mathbf{C}} \tag{1.26}$$

where the coefficients of the $1 \times K_{\text{win}}$ column vector $\tilde{\mathbf{C}}$ are computed using FT of the original $1 \times M$ signal array $\mathbf{C}$:

$$\left[\tilde{\mathbf{C}}\right]_j = \sum_{n=0}^{M-1} e^{in\varphi_j}c(n)\ , \quad j = 1, 2, ..., K_{\text{win}}\ . \tag{1.27}$$

Thus we express the amplitudes $\{d_k\}$ explicitly in terms of $\tilde{\mathbf{B}}_k$ and the time signal $c(n)$ as,

$$d_k^{1/2} = \sum_{j=1}^{K_{\text{win}}} \left[\tilde{\mathbf{B}}_k\right]_j \sum_{n=0}^{M-1} e^{in\varphi_j}c(n)\ . \tag{1.28}$$

An alternative expression for the amplitudes

As for normal eigenvalue solver, the eigenvalues are obtained variationally, while the eigenvectors are obtained in a non-variational way. Thus according to Eq. 1.26 the amplitudes d_k are generally much less accurate than the frequencies ω_k. In addition, given an eigenvector $\tilde{\mathbf{B}}_k$, Eq. 1.26 only makes use of the first half ($M = N/2$) of the time signal available and is not always the most accurate expression for the coefficient d_k that exists, especially for a narrow pole ω_k. As such a more accurate formula is derived for the narrow poles. First let us rewrite Eq. 1.6 in a more general form:

$$\begin{aligned} d_k^{1/2} &\equiv (\Upsilon_k|\Phi_0) = \left(\left[\hat{U}/u_k\right]^{n'} \Upsilon_k|\Phi_0\right) \\ &= u_k^{-n'}\left(\Upsilon_k|\hat{U}^{n'}\Phi_0\right) = u_k^{-n'}\sum_j \left[\tilde{\mathbf{B}}_k\right]_j (\Psi_j|\Phi_{n'}) \\ &= e^{n'\gamma}\sum_j \left[\tilde{\mathbf{B}}_k\right]_j \sum_{n=0}^{M-1} e^{in'\tau(\omega_k+i\gamma)} e^{in\tau\varphi_j} c_{n+n'} \ , \end{aligned}$$

where γ and n' are free parameters. We can now average the above expression over $n' = 0, 1, \ldots, M_{\text{aver}} - 1$ for an arbitrary M_{aver} between 1 and M,

$$\begin{aligned} d_k^{1/2} = &\frac{1-e^{-\tau\gamma}}{1-e^{-M_{\text{aver}}\tau\gamma}} \sum_j \left[\tilde{\mathbf{B}}_k\right]_j \\ &\times \sum_{n'=0}^{M_{\text{aver}}-1} \sum_{n=0}^{M-1} e^{in'\tau(\omega_k+i\gamma)} e^{in\tau\varphi_j} c_{n+n'} \ , \end{aligned} \tag{1.29}$$

where the averaging was done by weighting each term with $e^{-n'\gamma}$ (to eliminate the prefactor) and then normalizing the final result by $\left[\sum_{n'=0}^{M_{\text{aver}}-1} e^{-n'\gamma}\right]^{-1}$. Just like in Eq. 1.22 one of the two sums in Eq. 1.29 can be evaluated analytically (see Chapter 2). To eliminate the ambiguity in the choice of the free parameters in Eq. 1.29 for narrow poles ω_k (for which Eq. 1.29 is relevant), it suffices to stick with $M_{\text{aver}} = M$ and

$$\gamma = \begin{cases} -\text{Im}\{\omega_k\} \ , & \text{Im}\{\omega_k\} < 0 \\ 0 \qquad , & \text{Im}\{\omega_k\} > 0 \end{cases} .$$

For model signal or real signals with very high SNR, Eq. 1.29 does yield the amplitudes with more accuracy. However, it will lead to an ambiguous result if $M\tau|\mathrm{Im}\{\omega_k\}| \gg 1$, in which case the signal corresponding to these "broad" peaks should decay away very quickly and thus including longer signal to calculate their amplitudes would only deteriorate the accuracy. In these cases, Eq. 1.26 should be used.

1.1.3 FDM as a Spectral Estimator

Up to this point, FDM seems to be just a parameter estimator which can provide the parameter representation $\{w_k, d_k\}$ for a given FID by fitting it into Eq. 1.2. However, FDM can also be used as a spectral estimator. Once the parameters are available, one can easily obtain the spectral representation $I(w)$, formally defined as the infinite time Fourier integral,

$$I(\omega) = i\int_0^\infty C(t)e^{i\omega t}dt \ , \tag{1.30}$$

by simply substituting Eq. 1.2 into Eq. 1.30 and integrating the result analytically. The corresponding spectral estimate is here called the FDM *ersatz spectrum*,

$$I(\omega) \approx \sum_{k=1}^{K} \frac{d_k}{\omega_k - \omega} \ . \tag{1.31}$$

In FDM, some poles with extremely small imaginary part may occur (either due to the present of noise or real peaks), which leads to high spikes in the *ersatz* spectrum producing unfavorable results. Therefore, it is often useful to include a smoothing parameter Γ to improve the appearance of the spectra,

$$I(\omega) \approx \sum_{k=1}^{K} \frac{d_k}{\omega_k - \omega - i\,\Gamma} \ . \tag{1.32}$$

The absorption mode *ersatz* spectrum corresponds to

$$A(\omega) \approx \sum_{k=1}^{K} \mathrm{Im}\left\{\frac{d_k}{\omega_k - \omega - i\,\Gamma}\right\} \ . \tag{1.33}$$

In a single calculation, FDM can only obtain results for a particular small window, the construction of the overall spectrum requires one to combine the results from different spectral windows. To reduce the inaccuracies at the edges, the adjacent windows must overlap. One way to combine the results from overlapping windows is to scale the amplitudes of poles in each window, so that the contributions from all the windows that cover the same region add up to one. However, this seemingly obvious procedure often fails as it corresponds to a non-analytic transformation, which may destroy the very intimate relations between different terms in Eq. 1.31, based on mutual interferences and cancellations. A safer way to do this is first construct the corresponding spectra inside each window, then sum them up with appropriate weighting functions that add up to one. Such as

$$I(\omega) = \sum_r g^{(r)}(\omega) I^{(r)}(\omega) \ , \tag{1.34}$$

where r represents the r-th window, and $g^{(r)}(\omega)$ is an appropriate weight function which should satisfy $\sum_r g^{(r)}(\omega) = 1$. Any reasonable $g^{(r)}(\omega)$ should work well.

1.2 2D FDM

Given a 2D general complex valued time signal $c(\vec{n}) \equiv c(n_1\tau_1, n_2\tau_2)$, with $n_1 = 0, 1, ..., N_1 - 1, n_2 = 0, 1, ..., N_2 - 1$, where $\vec{n}$ is the time vector [†], defined on an equidistant time grid, we want to obtain a spectral representation of it. Ideally, we assume that the 2D signal can be fitted into following expression,

[†]Even though only 2D case is considered, the vector notations make the extension to more than 2D cases straightforward

$$c_{\vec{n}} = \sum_{k=1}^{K} d_k e^{-i\vec{n}\vec{\omega}_k} \equiv \sum_{k=1}^{K} d_k \exp\left(-in_1\tau_1\omega_{1k} - in_2\tau_2\omega_{2k}\right) \ , \tag{1.35}$$

where $\vec{\omega}_k \equiv (\omega_{1k}, \omega_{2k})$ are vectors of unknown complex frequencies, $\omega_{lk} = 2\pi f_{lk} - i\gamma_{lk}$, and d_k are unknown complex amplitudes. The total number of unknown complex parameters in the 2D line list $\{\vec{\omega}_k, d_k\}$ with K entries is $3K$. This is a 2D *harmonic inversion problem* (2D HIP). Just like 1D HIP, it can be cast into a linear algebraic problem, or more precisely, a family of generalized eigenvalue problems, by associating the 2D time signal to a double-time correlation function of a fictitious quantum system with two commuting non-Hermitian symmetric Hamiltonians $\hat{\Omega}_1$ and $\hat{\Omega}_2$ [4,9,11],

$$c(\vec{n}) = \left(\Phi_0 \middle| e^{-i\vec{n}\vec{\Omega}}\Phi_0\right) \equiv \left(\Phi_0 \middle| e^{-in_1\tau_1\hat{\Omega}_1 - in_2\tau_2\hat{\Omega}_2}\Phi_0\right) \ . \tag{1.36}$$

The Hamiltonians are assumed to have spectral representations,

$$\hat{\Omega}_l \Upsilon_{lk} = \omega_{lk}\Upsilon_{lk} \ , \quad l = 1, 2 \ . \tag{1.37}$$

Inserting Eq. 1.37 into Eq. 1.36, we can obtain

$$c(\vec{n}) = \sum_{k_1,k_2} d_{k_1k_2} e^{-in_1\tau_1\omega_{1k_1} - in_2\tau_2\omega_{2k_2}} \tag{1.38}$$

with

$$d_{k_1k_2} = T_{k_1k_2} b_{1k_1} b_{2k_2} \equiv (\Upsilon_{1k_1}|\Upsilon_{2k_2})(\Phi_0|\Upsilon_{1k_1})(\Phi_0|\Upsilon_{2k_2}) \tag{1.39}$$

Note that although we assume that the Hamiltonians $\hat{\Omega}_1$ and $\hat{\Omega}_2$ commute with each other, Eq. 1.37 does not assume that $\Upsilon_{1k} = \Upsilon_{2k}$, or equivalently, that $(\Upsilon_{1k}|\Upsilon_{2k'}) = \delta_{1k,2k'}$, as a "naive" approach would do. The purpose is to avoid the problem of finding a unique set of eigenvectors which simultaneously diagonalizes both Hamiltonians, as in cases of noisy signal or signal with degenerated poles such a unique set of eigenvectors does not necessarily exist. In other words, $T_{k_1k_2} = (\Upsilon_{1k_1}|\Upsilon_{2k_2})$ is not necessarily diagonal; nor can it necessarily be reduced to diagonal form by permutations. However, if we let $(\Upsilon_{1k}|\Upsilon_{2k'}) = \delta_{1k,2k'}$ in Eq. 1.39, the representation Eq. 1.38

boils down to the ideal representation of Eq. 1.35. Thus adopting representation of Eq. 1.38 covers the case of degenerate spectra and avoids the necessity of generating a unique set of eigenvectors $\{\Upsilon_k\}$, making the 2D FDM more robust and applicable to noisy time signals.

Matrix representations of the associated evolution operators $\hat{U}_l = e^{-i\tau_l n_l \hat{\Omega}_l}$ are also available only in terms of 2D time signals [‡]. When a 2D FT basis, define as,

$$|\Psi_j) = \sum_{n_1=0}^{M_1} \sum_{n_2=0}^{M_2} e^{i\vec{n}(\vec{\varphi}_j - \vec{\Omega})} |\Phi_0) \ , \tag{1.40}$$

is adapted, it is "locally complete" within the chosen spectral window. $\vec{\varphi}_j \equiv (\varphi_{1j}, \varphi_{2j})$, $j = 1, 2, \ldots, K$, is a 2D grid within the chosen spectral window. We can expand $|\Upsilon_{lk})$ in the local Fourier basis,

$$|\Upsilon_{lk}) = \sum_j \left[\tilde{\mathbf{B}}_{lk}\right]_j |\Psi_j), \ l = 1, 2 \ . \tag{1.41}$$

The operator eigenvalue problems in Eq. 1.37 can be then cast into two generalized eigenvalue problems,

$$\tilde{\mathbf{U}}_l \tilde{\mathbf{B}}_{lk} = u_{lk} \tilde{\mathbf{U}}_0 \tilde{\mathbf{B}}_{lk} \ , \quad l = 1, 2 \ . \tag{1.42}$$

The amplitudes $d_{kk'}$ are then obtained from the eigenvectors as

$$b_{lk} = \tilde{\mathbf{B}}_{lk}^{\mathrm{T}} \tilde{\mathbf{C}} \ , \tag{1.43}$$

where the coefficients of the $1 \times K_{\mathrm{win}}$ column vector $\tilde{\mathbf{C}}$ are computed using the following 2D FT of the original signal array $c(\vec{n})$:

$$\left[\tilde{\mathbf{C}}\right]_j = \sum_{n_1=0}^{M_{1j}-1} \sum_{n_2=0}^{M_j-1} e^{i\vec{n}\vec{\varphi}_j} c(\vec{n}) \ , \quad j = 1, 2, ..., K \ . \tag{1.44}$$

[‡]see ref. [11,13,28] for the expressions for computing $\tilde{U}^{(p)}$ matrices

The 2D spectral representation, which corresponds to a 2D Fourier integral of the signal, can then be written in terms of the Green's functions (or resolvent operators),

$$\begin{aligned} I(\omega_1,\omega_2) &= -\int_0^\infty dt_1 e^{i\omega_1 t_1}\int_0^\infty dt_2 e^{i\omega_2 t_2}\; C(t_1,t_2) \\ &= \Big(\Phi_0\,\Big|\,\hat{G}_1(\omega_1)\;\hat{G}_2(\omega_2)\;\Phi_0\Big) \qquad (1.45) \\ &= \sum_{k1,k2}\frac{d_{k1k2}}{(\omega_{1k}-\omega_1)(\omega_{2k}-\omega_2)}\;, \qquad (1.46) \end{aligned}$$

where an l-th Green's function can be represented in terms of the l-th eigenvectors and eigenvalues,

$$\hat{G}_l(\omega_l) \equiv \frac{1}{\hat{\Omega}_l-\omega_l} \equiv \sum_k \frac{|\Upsilon_{lk})(\Upsilon_{lk}|}{\omega_{lk}-\omega_l}\;. \qquad (1.47)$$

In addition, with Eq. 1.47, one can easily calculate the corresponding 1D projections in both dimension,

$$I_l(\omega_l) = \Big(\Phi_0\,\Big|\,\hat{G}_l(\omega_l)\;\Phi_0\Big) = \sum_{lk}\frac{b_{lk}^2}{(\omega_{lk}-\omega_l)}\;, \qquad (1.48)$$

where $b_{lk} \equiv (\Upsilon_{lk}|\Phi_0)$ as defined in Eq. 1.39.

Furthermore, it is often desirable to produce an absorption mode spectrum, which in the 1D case is obtained by simply taking the real part of the correctly phased FT spectrum. In the 2D case, purely phase modulated signals give rise to "phase-twisted" line-shapes. Neither the real or the imaginary part of 2D FT complex spectrum yields desired double absorption line-shape [14]. A double absorption spectrum can be only obtained by acquiring hyper-complex data [16], while in some other experiments, such as 2D-J, the hyper-complex signals are not available, leading to poor resolution even when the data sets are large. In the context of FDM, a double absorption spectrum is not much harder to construct than the conventional 2D complex spectrum (Eq. 1.45). One way of doing this is using following form,

$$A(\omega_1,\omega_2) = \sum_{k_1k_2}\mathrm{Re}\{d_{k_1k_2}\}\prod_{l=1,2}\mathrm{Im}\Big\{\frac{1}{\omega_{lk}-\omega_l}\Big\}\;, \qquad (1.49)$$

where we assume that the signal is correctly phased. However, this expression is not an unique representation, and is meaningful only when the different peaks with absorption shape are not overlapping too much, i.e., the interference effects are not significant.

Removing the artifacts by FDM averaging

Unfortunately, 2D FDM does not always work as well as 1D FDM. Spectra obtained from single 2D FDM calculation are never free from artifacts. The spectra would generally be unsatisfactory for relatively low SNR signals where the FT could still provide quite high resolution, given signals of sufficiently large size. The 2D FDM spectra are unstable with respect to the FDM parameters as well as small changes of the input signals. This instability manifests itself in numerous spurious spikes with random appearance. While the instability in the 1D FDM occurs for only "exotic" signals and can be eliminated by the use of multi-scale basis (see Chapter 2), in 2D FDM it is rather difficult to get rid of.

At this point it is still not absolutely clear what causes the instability in the 2D FDM calculations. One explanation [28] is based on the comparison between the 1D and 2D methods. In the 1D FDM a signal of size N leads (in the Krylov basis) to a generalized eigenvalue problem of rank $M_{\text{Krylov}} = N/2$, which, in turn, yields $N/2$ pairs of (ω_k, d_k), i.e. totally N parameters. This means that the solution of the HIP, Eq. 1.2, is unique with the total number of equations exactly matching the total number of unknowns. In the 2D case the situation is different. In the Krylov basis the total rank of the U-matrices is $M_{\text{Krylov}} = N_1 N_2/4$, resulting in $N_1 N_2/4$ frequencies ω_{lk} for each generalized eigenvalue problem, Eq. 1.11. If according to the form of Eq. 1.35 we assume the total number of 2D Lorentzian peaks (each characterized

by two frequencies ω_{1k} and ω_{2k} and an amplitude d_k) to be M_{Krylov}, we will have to deal with an over-determined problem with totally N_1N_2 equations and $\frac{3}{4}N_1N_2$ unknowns. Therefore for a general 2D array c_{n_1,n_2} of fixed size the exact solution of the 2D HIP is, strictly speaking, not obtainable by FDM. When applying FDM we implicitly assume that the data set can be fit by the parametric form of Eq. 1.35, i.e. we assume that this data is not generic. That is, the Lorentzian form cannot be satisfied exactly for general noisy signals, using the number of parameters consistent with the FDM procedure. The above explanation does not pretend to be absolutely correct but it, at least, confirms that there is something wrong with the 2D HIP.

One simple solution to overcome this is to take advantage of the randomness of the artifacts appearing in the spectrum when the signal size is changed [10,11]. When sufficiently many FDM spectra calculated using different N_1 are summed together, these artifacts magically average out. We call it the *signal size averaging*. It is applicable only in situations where the signal is sufficiently long in at least one dimension such as the running time. One obvious drawback of the method is that N_{FDM} (rather than one) FDM calculations have to be performed, significantly increasing the overall numerical effort. The second serious drawback is that an averaged spectrum does not correspond to a compact parameter list. It is the latter reason though which explains the averaging phenomenon as the huge number of parameters from different FDM calculations used to construct the averaged spectrum eliminate the overdeterminicity problem of a single solution of the 2D HIP.

There is a more elegant way to perform averaging. Instead of changing the signal length we exploit the great sensitivity of the output spectrum to small variations of the input signal of fixed size. We first perturb the signal by adding small amount of pseudo-noise and then sum up resulted the *ersatz* spectra. We call it a *pseudo-noise averaging* procedure. Note, that the signal size averaging has essentially no

free parameter and is limited by the maximum signal size, while the pseudo-noise averaging uses arbitrary number of samples with an arbitrary noise amplitude λ, which usually has to be determined experimentally. Furthermore, the pseudo-noise averaging can be implemented at the stage of applying Eq. 1.11 using the fixed U-matrices computed once from the original signal because that U-matrices are linear functions of the input signal $c_{\vec{n}}$, which will lead to some simplification of the averaging procedure [28].

Chapter II

Multi-Scale FDM for Spectral Analysis of Noisy Signals

2.1 Introduction

As described in Chapter I, FDM can be used both as a parameter estimator and spectral estimator. However, Use of a complicated non-Fourier spectral estimator can be justified only if the result is at least as reliable as the Fourier spectrum of the same truncated signal and, at the same time, may deliver a higher resolution as one expects from a high resolution method. This is usually the case (some examples can be found in refs. [3,7]). As long as the two key assumptions, i.e., Eq. 1.2 and the block diagonalizability of the U matrix in the Fourier window basis, are well satisfied, FDM can provide a high fidelity line list and thus an accurate spectral estimate using Eq. 1.31. However, when the signal has a low signal/noise ratio (SNR) and/or when its spectrum has some significant non-localized global spectral features the line list may contain some poorly converged poles and result in inaccurate *ersatz spectrum*. Fig. 1 shows such a case, in which the signal used is the first increment of a 2D HSQC NMR signal of the steroid progesterone [6] with many overlapping multiplets and low signal/noise ratio. For $N = 2000$ the FT spectrum is converged in the sense that taking a longer signal does not improve the resolution further, but only increases the noise level. Although one may be interested in a parametric quantification of this spectrum using Eq. 1.2, clearly, in this regime the use of a non-Fourier method, as a spectral estimator toe improve the FT resolution, is hardly justified. However, to demonstrate the point of the above discussion we apply FDM to the same data. The resulting FDM *ersatz* spectrum is distorted in some regions and appears to be sensitive to the parameters used, such as window size, number of the Fourier basis functions K_{win}, etc. We will refer to this problem as the "instability" problem in the rest of this chapter.

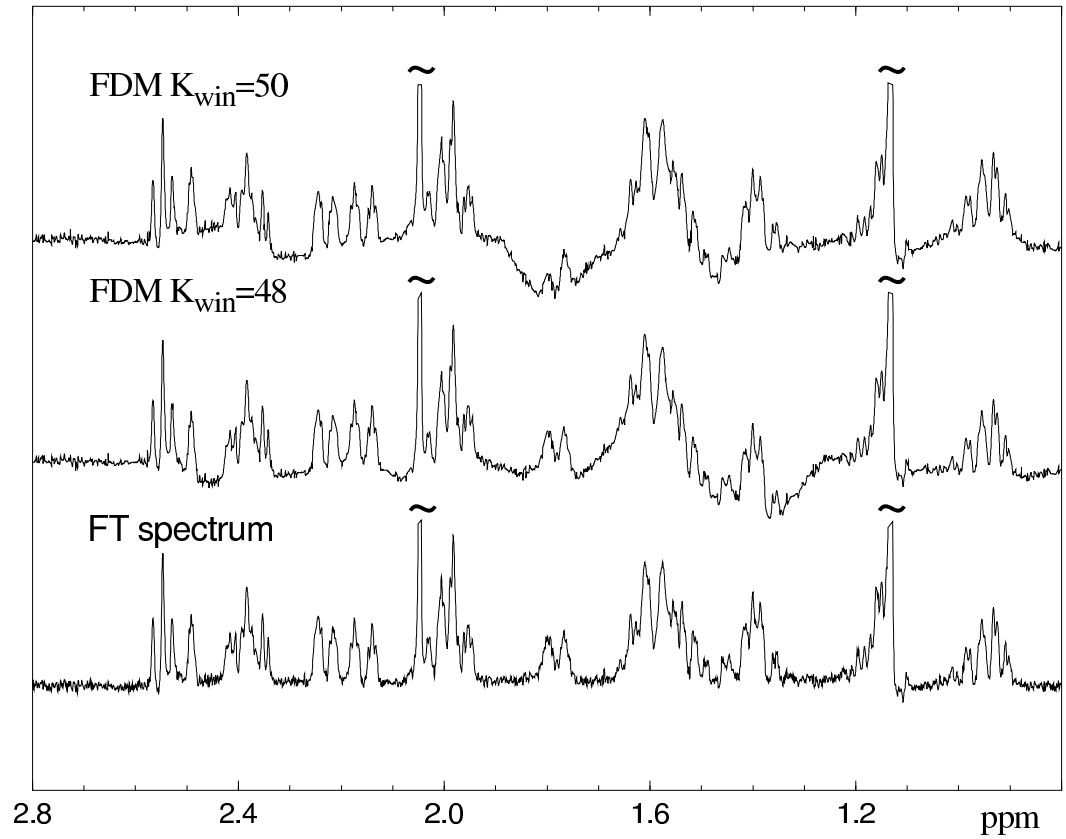

FIG. 1. *Spectra obtained from a noisy 1D NMR signal of length* $N = 2000$ *and spectral width* $SW = 4$ *ppm (2kHz) using two different methods, FT with an appropriate apodization (bottom) and FDM (the upper two traces). The FDM ersatz spectra used slightly different numbers,* $K_{\rm win} = 48$ *and* $K_{\rm win} = 50$*, of the Fourier basis functions per window, corresponding to bandwidths 0.192 ppm and 0.2 ppm, respectively. Note that a multi-window approach (see text) was used to construct the overall FDM spectra.*

Qualitatively, the origin of this instability is as following. We use narrow band Fourier basis functions, Eq. 1.18, which are highly localized in the frequency domain. On one hand, this is a big advantage of using the Fourier basis, on the other hand, in the presence of noise, a narrow band basis is inadequate to represent a broad spectral feature that is not localized in a single window, as each basis function $|\Psi_j)$ is "locked"

on the noise peaks that appear close to φ_j and cannot "see" the peaks that are far away. For example, if there exists a broad peak that centers outside of the current spectral window but tails into the window, the narrow band Fourier basis would not be enough to accurate represent the contribution of this broad peak. Thus, with the narrow band Fourier basis only, we may have some ambiguity in reproducing the broad spectral features or the baseline, and this is the source of instability. Obviously, such instability can sometimes be reduced by using larger windows. However, increasing the basis size does not always work, and even when it does, it is impractical due to very unfavorable scaling of the computational cost for an eigenvalue solver. Therefore, we need to improve the algorithm to make it robust and reliable even for such kind of noisy signals, but avoid the computationally expensive solutions. In this chapter, we will introduce some primitive method and a more consistent method, multi-scale FDM, to solve this problem.

The rest of this chapter is organized as followings. In Section 2.2 three primitive hybrid methods using FT and/or FDM are discussed. Section 2.3 presents *Multi-Scale FDM* with some model and practical examples, including NMR and IR spectra. A multidimensional extension of the method is given in Section 2.4. At last, a summary of this chapter given in Section 2.5. The derivation of matrix elements of the U-matrices for the multi-scale FDM and some numerical implementation notes are given in the appendixes.

2.2 Some Primitive Hybrid Methods

A discrete Fourier transform (DFT) of a truncated data provides a uniformly converged spectral estimate, practically, regardless of the signal/noise ratio, the dis-

tribution of the spectral peaks and their lineshapes and widths. This property can be attributed to both the advantages and disadvantages of DFT. Ideally, a high resolution method for solving the harmonic inversion problem, Eq. 1.2, such as FDM, often leads to significant resolution enhancement, especially, for narrow and/or isolated peaks. In addition, the high sensitivity of the data acquisition, i.e., high signal/noise ratio, can effectively be converted to high spectral resolution. However, as discussed in the previous section, due to imperfections of a parametric fit of a real noisy data the line list may contain spurious or poorly converged entries, which usually correspond to broad spectral features and lead to distortions in the FDM *ersatz spectrum*. In this section we discuss several simple methods to correct the imperfections of the FDM *ersatz spectrum* by more efficient use of the signal available.

2.2.1 Hybrid FT + FDM

The fact that the signal is truncated limits the highest resolution we are able to achieve by DFT. To illustrate this, we rewrite Eq. 1.30 as following,

$$I(\omega) = i\int_0^{t_{\max}} C(t)e^{i\omega t}\,dt + i\int_{t_{\max}}^{\infty} C(t)e^{i\omega t}\,dt \tag{2.1}$$

In conventional Fourier spectral analysis only the first term is available. It is the absence of the second term, i.e., the tail part of FT, that limits the Fourier resolution. If somehow this second integral can be estimated and added to the first term, one can improve the resolution. For example, in most implementations of the Linear Prediction (LP), the signal is extrapolated beyond the maximum available time $t_{\max}$ and then Fourier transformed (see, e.g., refs. [19–22]). Clearly, this can also be done by FDM, as the parameters $\{\omega_k, d_k\}$ can be used to extrapolate the signal to infinite length. Note, yet, that the straightforward use of Eq. 2.1 will enhance the truncation artifacts. A more appropriate form of Eq. 2.1 is given in ref. [2] where the infinite time

integral is split into two contributions by inserting the identity $1 = f(t) + [1 - f(t)]$ with $f(t)$ being some smoothed theta function that vanishes for $t > t_{\max}$:

$$I(\omega) \approx i \int_0^{t_{\max}} e^{it\omega} f(t) C(t) dt + i \int_0^{\infty} e^{it\omega} [1 - f(t)] \sum_k d_k e^{-it\omega_k} dt \ . \tag{2.2}$$

The first integral is computed by DFT, the second, dominated by the long time ($t \geq t_{\max}$) contributions so that for its evaluation one can retain only the narrow poles ω_k, that are computed accurately by FDM. Furthermore, it can be computed efficiently for an appropriate choice of $f(t)$ as the integrand is some analytically known function.

2.2.2 Hybrid FDM+FT

Unlike the previous hybrid method, where FDM was used to enhance the resolution of finite FT, a *vice versa* strategy is to correct the imperfections of the FDM *ersatz spectrum*, given by Eq. 1.2, using post-processing by DFT [3].

One can always estimate how well the original signal is fit by the form of Eq. 1.2 by examining the residual signal,

$$C_{\rm res}(t) = C(t) - \sum_k d_k e^{-it\omega_k} \ . \tag{2.3}$$

In the context of FDM, the FT spectrum of $C_{\rm res}(t)$ in the spectral region of interest measures the imperfections of the FDM line list. To correct the *ersatz spectrum* obtained by Eq. 1.31, we can apply FT to the residual signal,

$$I(\omega) \approx \sum_k \frac{d_k}{\omega_k - \omega} + i \int_0^{t_{\max}} e^{it\omega} f(t) C_{\rm res}(t) dt \ , \tag{2.4}$$

with $f(t)$ being some appropriate apodization function. By adding FT of residual signal to the FDM *ersatz spectrum*, we actually compensate the imperfections that

occur during the fitting. A perfect fit will result in a zero residual spectrum which will not affect the FDM spectrum. However, in some situations, the residual spectrum, appearing as a smooth baseline distortion, could be noticeable.

2.2.3 Hybrid FDM+FDM

As pointed out in Section 2.1, it is probably the presence of global features that causes the "instability" problem. If FDM can somehow take "good" care of both the global (broad) and local (narrow) features, we should be able to improve the performance of FDM. Here we propose another hybrid method in which the global and local features are treated separately. That is, one can generate two line lists from C(t), a *coarse line list* and *narrow band line list*, that will result in a correct spectrum when used with Eq. 1.31. This can be done in two steps: First, FDM is applied to obtain the global fit of a short part of $C(t)$ in terms of the coarse line list, $\{\omega_k^{(\mathrm{c})}, d_k^{(\mathrm{c})}\}$, which generally constitutes of broad poles and can therefore describe well the broad spectral features (in practice, only the broad poles should be retained). At the second step FDM is applied to the residual signal,

$$C_{\mathrm{res}}(t) = C(t) - \sum_k d_k^{(\mathrm{c})} e^{-it\omega_k^{(\mathrm{c})}} \ , \tag{2.5}$$

using all the available data, to create the narrow band line list $\{\omega_k^{(\mathrm{l})}, d_k^{(\mathrm{l})}\}$ in the spectral region of interest. $\omega_k^{(\mathrm{l})}$ are generally much narrower than $\omega_k^{(\mathrm{c})}$, because by subtracting the contribution of broad poles in Eq. 2.5 only narrow features will be left in the residual signal $C_{\mathrm{res}}(t)$. The overall spectrum in the specified frequency window is then estimated by using both line lists,

$$I^{(\mathrm{l})}(\omega) \approx \sum_k \frac{d_k^{(\mathrm{c})}}{\omega_k^{(\mathrm{c})} - \omega} + \sum_k \frac{d_k^{(\mathrm{l})}}{\omega_k^{(\mathrm{l})} - \omega} \ . \tag{2.6}$$

In this approach instability due to the necessity to deal with both the broad and narrow spectral features does not occur since they are fit separately in two different steps.

2.2.4 Performance and Problems

All of the above three hybrid methods are quite similar in both the computational efficiency and robustness, and show only minor differences whenever construction of a 1D spectrum is of interest. For example, in certain regimes both hybrid methods FT+FDM and FDM+FT could result in some residual Gibbs oscillations (albeit very small) which are hard to eliminate completely. Those never occur in the hybrid FDM+FDM procedure, although in the latter the total number of parameters in the overall line list is not quite consistent with the total size of the data, i.e. the data is over-fit. If some poorly converged poles with large amplitudes happen to occur in the first step, the reconstruction and subtraction step will effectively introduce some extra noise to the signal. In addition, none of these hybrid methods can provide a line list which is consistent with the *ersatz spectrum* obtained, which could be desirable in many cases.

A major drawback of the hybrid methods actually occurs when we try to generalize them to the multidimensional cases, where the spectral construction has to be somewhat more complicated than in the 1D case. Besides, a double-absorption spectrum cannot be obtained from a purely phase modulated 2D signal by FT, which excludes the hybrid methods that require FT from our consideration. To conclude, it may not be appropriate to take care of global and local features separately, especially in a multidimensional signal processing.

2.3 Multi-Scale FDM

In this section, a more consistent method to solve the "instability" problem which we call *Multi-Scale FDM* will be presented. As mentioned above, the instability in the FDM line list may occur because localized basis functions do not describe correctly the spectral peaks that are broader than the width of the spectral window. To take into account the global features but avoid the use of a big Fourier basis we need to add to our narrow band and dense window basis some sparse *coarse* (i.e., delocalized) basis functions. Since the broad peaks do not require high resolution we do not need many of such coarse basis functions. We also want to minimize the number of coarse basis functions with the condition that the non-localized features that may affect the local spectral analysis are represented adequately, which can be achieved by choosing the most efficient coarse basis distributions.

2.3.1 Theory

Given that the farther away from the current window, the less significant the effect of a broad spectral feature to the local analysis, the coarse basis could be chosen such that the spacing between the adjacent coarse basis functions and, accordingly, their bandwidth, monotonically increase with respect to the distance between the center of the basis function (φ_j) and the spectral window of interest. Thus only the features, which are broad enough to affect the current window, will be captured by the coarse basis. Here the local density of the basis functions is defined as

$$\rho_j = \frac{2\Delta\varphi_{\min}}{|\varphi_{j+1} - \varphi_{j-1}|} \tag{2.7}$$

where $\Delta\varphi_{\min} = 2\pi/\tau M_{\max}$ is determined by the spacing between the narrow band Fourier basis functions. The Fourier length should be scaled accordingly to the local density using $M_j = \rho_j M_{\max}$, which makes the bandwidth of the basis functions consistent with the basis density. For a given small spectral window we can construct a multi-scale basis, which contains $K_{\vec{\varphi}\text{win}}$ narrow band Fourier basis functions localized in the window and K_{c} coarse basis functions spread over a wide spectral range:

$$|\Psi_j) = \sum_{n=0}^{M_j-1} e^{in\varphi_j}|\Phi_n), \;\; j = 1, 2, \ldots, K = K_{\text{win}} + K_{\text{c}} \tag{2.8}$$

with the Fourier length M_j depending on j: $M_j = M_{\max}$ for the narrow band, and $M_j = M_{\max}\,\rho_j$, for the coarse basis functions.

The $\mathbf{U}$ matrix representations can then be evaluated in terms of the time signal. Here we derive an efficient formula for evaluating the off-diagonal matrix elements $\left[\mathbf{U}^{(p)}\right]_{jj'}$. The corresponding expression for the diagonal ones is the same as that previously derived in ref. [3]. Using the definition of multi-scale FT basis $|\Psi_j)$ and $|\Psi_{j'})$, Eq. 2.8, and the ansatz of Eq. 1.3 we obtain

$$\begin{aligned}
\left[\mathbf{U}^{(p)}\right]_{jj'} &= \sum_{n=0}^{M_j-1}\sum_{n'=0}^{M_{j'}-1} e^{in\tau\varphi_j} e^{in'\tau\varphi_{j'}} \left(\Phi_n \left| U^{(p)} \Phi_{n'}\right.\right) \\
&= \sum_{n=0}^{M_j-1}\sum_{n'=0}^{M_{j'}-1} e^{in\tau\varphi_j} e^{in'\tau\varphi_{j'}} c(n+n'+p) \\
&= \sum_{n=0}^{M_j-1}\sum_{n'=0}^{M_{j'}-1} e^{i(n+n')\tau\varphi_j} e^{in'\tau(\varphi_{j'}-\varphi_j)} c(n+n'+p)\;.
\end{aligned} \tag{2.9}$$

Unlike the case corresponding to a uniform Fourier basis [3], here M_j and $M_{j'}$ do not always equal to each other, which makes this expression a little bit more complicated. However, using the strategy of ref. [3], we can still simplify the numerically expensive double sum. First, by substituting $l = n + n'$, and assuming $M_j < M_{j'}$, we break it into three terms,

$$\sum_{n=0}^{M_j-1}\sum_{n'=0}^{M_{j'}-1} = \sum_{l=0}^{M_j-1}\sum_{n'=0}^{l} + \sum_{l=M_j}^{M_{j'}-1}\sum_{n'=l-(M_j-1)}^{l} + \sum_{l=M_{j'}}^{M_{j'}+M_j-2}\sum_{n'=l-(M_j-1)}^{M_{j'}-1}\;.$$

Then by evaluating analytically the summations over n', we can replace each term by single summations. After some manipulations, we obtain

$$\begin{aligned}\left[\mathbf{U}^{(p)}\right]_{jj'} = \frac{1}{1-e^{i\tau(\varphi_{j'}-\varphi_j)}} \Bigg\{ & \sum_{n=0}^{M_j-1} e^{in\tau\varphi_j} c(n+p) \\ & - e^{i\tau(\varphi_{j'}-\varphi_j)} \sum_{n=0}^{M_{j'}-1} e^{in\tau\varphi_{j'}} c(n+p) \\ & + e^{-i(M_j-1)\tau(\varphi_{j'}-\varphi_j)} \sum_{n=M_j}^{M_j+M_{j'}-2} e^{in\tau\varphi_{j'}} c(n+p) \\ & - e^{iM_{j'}\tau(\varphi_{j'}-\varphi_j)} \sum_{n=M_{j'}}^{M_{j'}+M_j-2} e^{in\tau\varphi_j} c(n+p) \Bigg\} \end{aligned} \tag{2.10}$$

Note that the final result is symmetric with respect to the interchange of indices j and j' as it should be. Also note, that for $M_j = M_{j'}$ Eq. 2.10 boils down to the formula previously derived [3]. It can then be rewritten in a compact form, which can be easily generalized to a multi-dimensional case,

$$\left[\mathbf{U}^{(p)}\right]_{jj'} = \hat{S} \sum_{\sigma=0,1} \frac{e^{i\sigma[M_{j'}(\varphi_{j'}-\varphi_j)+\pi]}}{1-e^{i(\varphi_{j'}-\varphi_j)}} \times \sum_{n=\sigma M_{j'}}^{\sigma(M_{j'}-1)+M_j-1} e^{in\varphi_j} c(n+p) \ , \tag{2.11}$$

where $\hat{S}$ is the symmetrization operator over the subscripts j and j', as defined in Eq. 1.24. For the diagonal matrix elements, $\varphi_j = \varphi_{j'}$, the expression is equivalent to that previously derived [3]:

$$\left[\mathbf{U}^{(p)}\right]_{jj} = \sum_{n=0}^{2M_j-2} (M_j - |M_j - n - 1|) e^{in\varphi_j} c(n+p) \ . \tag{2.12}$$

Once the U-matrices are available in this new basis, one can solve the generalized eigenvalue problem Eq. 1.11 to obtain the eigenvalues u_k and eigenvectors $\mathbf{B}_k$. Due to Eqs. 1.12 and 2.8 the latter yield the amplitudes with

$$\sqrt{d_k} = \sum_{j=1}^{K} [\mathbf{B}_k]_j \sum_{n=0}^{M_j-1} e^{in\varphi_j} c(n) \tag{2.13}$$

As pointed out previously in Chapter 1.2.2, given the eigenvectors $\mathbf{B}_k$, Eq. 2.13 may not provide the highest accuracy for the coefficients d_k, especially those corresponding

to narrow poles ω_k. A more general expression can be obtained following the same procedure,

$$\sqrt{d_k} = \frac{1-e^{-\tau\gamma}}{1-e^{-M_{\rm aver}\tau\gamma}} \sum_j [\mathbf{B}_k]_j \times \sum_{n'=0}^{M_{\rm aver}-1} \sum_{n=0}^{M_j-1} e^{in'\tau(\omega_k+i\gamma)} e^{in\tau\varphi_j} c(n+n') \ , \tag{2.14}$$

where formally γ and M_{aver} are free parameters. This double sum is equivalent to that in Appendix I (Eq. 2.9) with $p = 0$ and $\varphi_{j'} = \omega_k + i\gamma$ and therefore can be simplified using the result of Eq. 2.10 or, equivalently, Eq. 2.11.

We found by numerical experimentations that Eq. 2.14 improves the accuracy for the amplitudes, compared to that of Eq. 2.13, if ω_k is sufficiently narrow, i.e., $|\mathrm{Im}\{\omega_k\}|$ is small. In this case an appropriate choice for the free parameters is $M_{aver} = M_{\max}$ and $\gamma = -\mathrm{Im}\{\omega_k\}$ for $\mathrm{Im}\{\omega_k\} < 0$ and $\gamma = 0$, otherwise. For broad poles, especially those captured by coarse basis, their contribution to the signal decays very quickly and usually they only contribute to the beginning part of the signal. As such, taking the second half of the signal into account by using Eq. 2.14 will only make the results less accurate. Therefore, Eq. 2.13 should be used for broad poles. A good criteria to distinguish "broad" and "narrow" poles would be the smoothing parameter Γ used to plot the *ersatz spectrum* in Eq. 1.32, which is usually $0.1 \sim 0.2$ of FT resolution.

Fig. 2 shows an example of such a basis set for a particular window together with the FDM ersatz spectrum obtained using this basis and plotted, intentionally, in a wide spectral range. As expected, fine features are captured inside the window where dense and narrow band basis functions are used, and only coarsely resolved features appear in the region outside this window. Furthermore, the spectral resolution decreases smoothly in the directions away from the window, so there are no edge effects associated with the local spectral analysis. This makes it easier to combine the results of different windows to construct the overall spectrum. More importantly, with the

presence of coarse basis, the spectral features outside of the window are represented with relatively lower resolution, so that the base line inside the window is now very stable, which means that our first purpose of removing the "instability" problem is achieved.

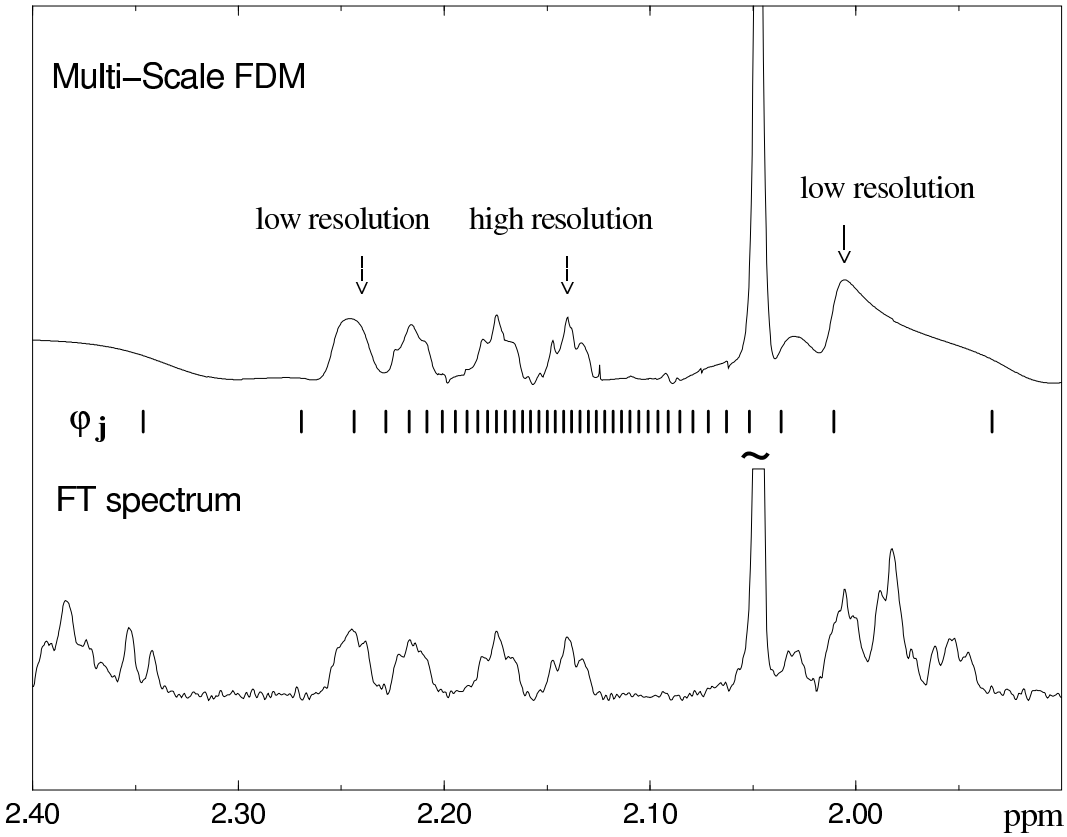

FIG. 2. *An example of a multi-scale basis set and the spectrum obtained using this basis for the same signal used in Fig. 1.* $K_{\rm win} = 10$ *narrow band and* $K_c = 20$ *coarse basis functions (indicated by an impulse at each* φ_j*) were used. The coarse functions are distributed non-uniformly according to the displacement from the window (see text).*

2.3.2 Some Aspects of Numerical Implementations

A comment must be made on how to calculate the discrete Fourier sums for all j and j' in Eq. 2.10 efficiently. The first two sums need to be computed only once for every j. The other two sums depend on both indices j and j', and might seem numerically expensive. Here we describe an algorithm which scales as $M_{\max} \times K_{\text{win}}$ for all the matrix elements of $\mathbf{U}^{(p)}$ rather than $M_{\max} K_{\text{win}}^2$ as one can think. Thus the numerical effort of evaluating the U-matrices in a multi-scale Fourier basis is similar to that of the original version of FDM.

For convenience, we introduce the notation:

$$g_j^{(p)}(M) \equiv \sum_{n=M+1}^{M+M_j-1} e^{in\tau\varphi_j} c(n+p) \ .$$

Since $g_j^{(p)}(M_{\max}-1)$ only depends on φ_j, it can be evaluated once and stored in an array for later use. Now given $g_j^{(p)}(M_{\max})$, one can obtain $g_j^{(p)}(M_{j'})$ recursively for all $M_{j'} < M_{\max}$ according to

$$\begin{aligned} g_j^{(p)}(M-1) = g_j^{(p)}(M) &+ e^{iM\tau\varphi_j} c(M+p) \\ &- e^{i(M+M_j-1)\tau\varphi_j} c(M+M_j-1+p) \ . \end{aligned}$$

Finally, another trivial point is that there is no need in evaluating the Fourier sums in Eq. 2.10 for $p=1$, once they have been computed for $p=0$ as there is always a simple relation between these two. For example,

$$\sum_{n=0}^{M} e^{in\tau\varphi} c(n+1) = e^{-i\tau\varphi} \left[\sum_{n=0}^{M} e^{in\tau\varphi} c(n) - c(0) \right] e^{iM\tau\varphi} c(M+1) \ .$$

2.3.3 A double-scale Fourier Basis

Our second purpose is to find out the most efficient coarse basis distribution which would require minimum computational efforts to get similarly reliable result. We found, again by numerical experiment, that for the simplest realization of a multi-scale Fourier basis one can consider just two scales with $M_j = M_{\max}$, for the narrow band window basis, and $M_j = M_c \ll M_{\max}$, for the coarse basis, corresponding to having two equidistant grids with spacings, $\Delta\varphi_{\min} = 2\pi/\tau M_{\max}$ and $\Delta\varphi_c = 2\pi/\tau M_c$, respectively. At first look, this double scale distribution may not sound as well as the real "multi-scale" basis with smoothly decaying basis density. However, numerical experiments showed that such a basis distribution is sufficient to get "good" results for most circumstances, while there may always exist some cases that require a profound basis distribution.

Unlike the example shown in Fig. 2 which might seem to be a little complicated, this simplifies the calculation of the U-matrix elements (see Appendix I). Furthermore, the size of coarse basis can be further reduced (or contracted) by keeping only those basis functions $|\Psi_j)$ for which no significant peaks appear in a low resolution Fourier spectrum around φ_j. Numerical implementation of this "adaptive coarse basis" idea will require pre-applying DFT or FDM to a short signal to get a low resolution picture. It is also worth noting that the use of a double scale basis is reminiscent to the hybrid FDM+FDM, although in the latter the two diagonalizations are decoupled, while in the more consistent approach of this section only one diagonalization is performed but using the hybrid double-scale basis. The examples shown in next example section are all obtained with the double-scale FDM.

2.3.4 Multi-Scale Fourier Basis Using Complex Grid

There is an even simpler implementation of the multi-scale FDM which does not require any of the new formula derived previously in this section, in which instead of the real frequency grid $\{\varphi_j\}$ (Eq. 1.18), a list of complex values $\varphi_j^{(c)}$ are used. The real parts are just $\{\varphi_j\}$. Let's Eq. 1.18 are rewritten as,

$$|\Psi_j) = \sum_{n=0}^{M_{\max}-1} e^{in\varphi_j}\, e^{-n\,\mathrm{Im}\varphi_j^{(c)}}\, |\Phi_n) \;, \tag{2.15}$$

Note that if $\mathrm{Im}\varphi_j^{(c)} = 0$ this new definition is the same as Eq. 1.18. When $\mathrm{Im}\varphi_j^{(c)} > 0$, the second exponential acts as a FT weight function, and changes the "effective FT length". Thus adjusting the imaginary part of the complex grid points $\varphi_j^{(c)}$ will have the same effect as directly adjusting the FT length like what is done in Eq. 2.8. The relation between $\mathrm{Im}\varphi_j^{(c)}$ and M_j is given as,

$$\sum_{n=0}^{M_{\max}-1} e^{-n\,\mathrm{Im}\varphi_j^{(c)}} = M_j \;. \tag{2.16}$$

This equation can be solved analytically by first substituting the summation by a integral and solve the simplified equation. The result can then be expanded in Taylor series and approximated by

$$\mathrm{Im}\varphi_j^{(c)} = \begin{cases} \frac{1}{t} + x - x^2 + 1.5x^3 & \text{if } t > 0.685 \\ 2.82(1-t) & \text{if } t < 0.685 \end{cases} \;, \tag{2.17}$$

where $t = M_j/M_{\max}$, $x = \exp(1/t)$, and M_j has the same dependence on basis distribution as previously defined. With such a definition of multi-scale FT basis, we can use the formulas of the single scale FDM by simply substituting the real grid φ_j by the complex one. This will simplify the implementation of the 2D or higher dimensional multi-scale FDM. Numerical experiments demonstrated that the performance of the complex-grid multi-scale FDM is similar to that of the original implementation of the multi-scale FDM.

2.3.5 Some Numerical Examples

Fig. 3 shows some spectra obtained with the double-scale basis. The use of a coarse basis does improve the appearance of the spectrum significantly, even when very few basis vectors is used. Furthermore, due to the removal of the edge effects by

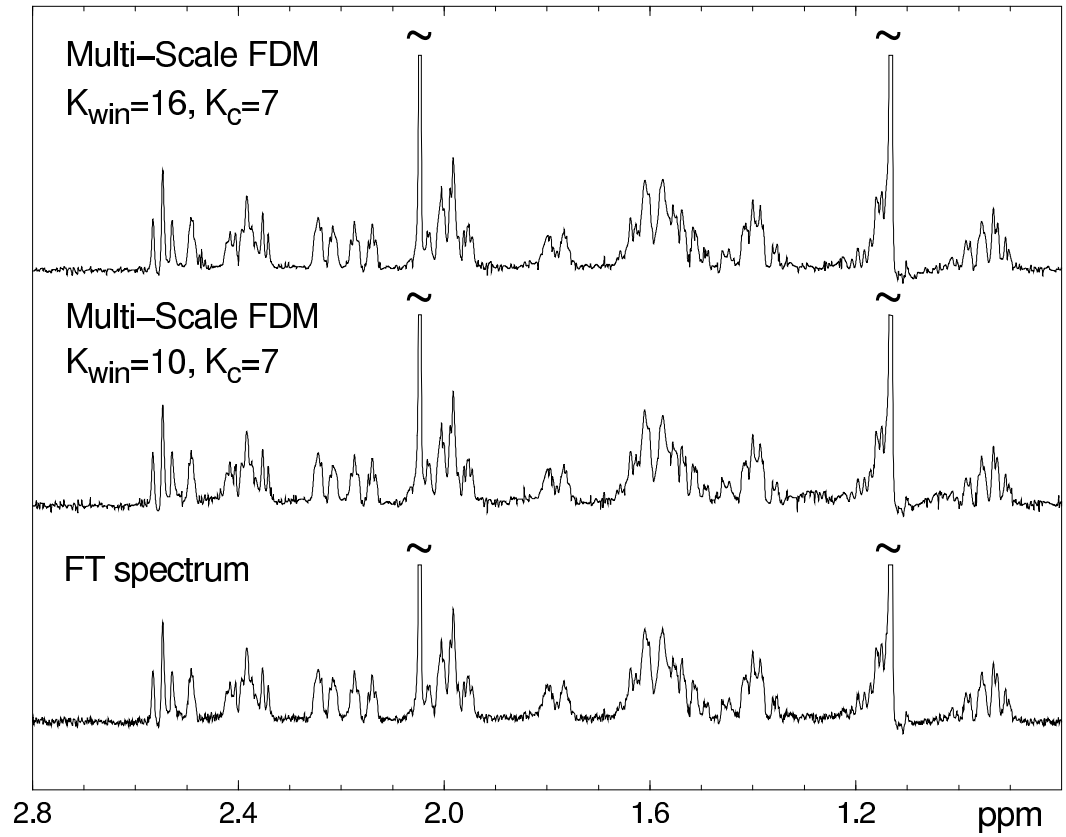

FIG. 3. *A comparison of FT and multi-scale FDM ersatz spectra generated by Eq. 1.31. The overall basis as small as* $K_{\rm win} + K_c = 10 + 7 = 17$ *still gives a reasonable spectrum. Further increase of the window basis to* $K_{\rm win} = 16$ *leads to an absolutely converged result in that it is stable and insensitive to the FDM parameters used, such as basis size, window position etc.*

the latter, the size of the narrow band basis could be very small as well, compared to the previous single-scale version of FDM. As such, for the example considered here about $K_c = 7$ coarse basis functions, retained after the contraction procedure, and $K_{\rm win} \geq 10$ window basis functions were needed to obtain well converged ersatz spectra.

The example of Fig. 3 demonstrates the reliability and robustness of the multi-scale FDM. The next example in Fig. 4 shows that under even more extreme conditions it is still as stable as the Fourier spectrum but can deliver a higher resolution than both the Fourier spectrum and the previous single-window version of FDM. We considered the same NMR signal to which, in the region with no genuine NMR lines, we added artificially some very broad Lorentzian lines to simulate a huge background spectrum and some very narrow lines. For this extreme case, the single-scale FDM does not work well even when a quite big window basis is implemented. For example, for signal length $N \sim 2000$ and $K_{\rm win} \sim 200$ window basis functions the spectrum envelop is not reproduced correctly. Moreover, in this case the results appeared to be quite sensitive to the input parameters, such as a slight shift in the window position. While reproducing the background spectrum is not a problem for the Fourier spectrum it cannot resolve the doublet made out of two narrow, equal in height and closely spaced Lorentzian lines. Quite surprisingly, the multi-scale FDM with just $K_{\rm win} + K_c = 4 + 10 = 14$ basis functions per window reproduces all the relevant spectral features quite accurately. Moreover, the doublet is now much better resolved than in both the single-scale FDM and FT spectra.

Finally, Fig. 5 presents an IR spectrum. The interferogram contained 4744 data points that were processed by both FT and multi-scale FDM to generate the absolute value spectra $|I(\omega)|$. The FT spectrum is very hard to interpret and, probably, hard to quantify by conventional means as the peaks are not quite narrow and both the

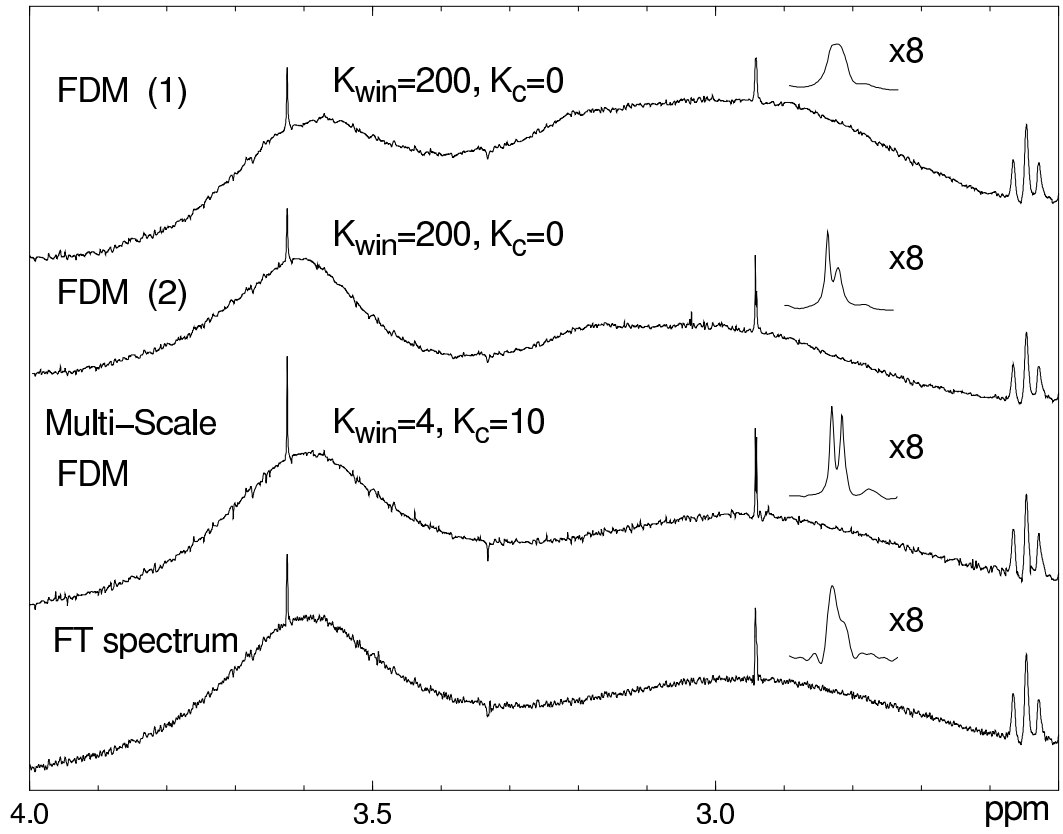

FIG. 4. *This example shows the spectra of an artificially made signal (see text) processed by three different methods, FDM (single-scale FDM), multi-scale FDM and FT. The spectrum marked with FDM (2) was obtained with the same parameters as FDM (1) but the position of the window was slightly shifted. The instability in both representing the background spectrum and resolving the fine features (the doublet) occurs even with* $K_{\rm win}$ *as large as 200 basis functions (corresponding to 0.88 ppm spectral window). The doublet is not resolved in the FT spectrum either due to the uncertainty relation, although FT reproduces the spectrum envelop correctly. The result obtained by the multi-scale FDM with just* $K_{\rm win} + K_c = 4 + 10 = 14$ *basis functions is superb in all respects and required minimal computational effort.*

overlapping effects and the interference with the background are significant. Unlike

the FT case, the FDM peaks are generally much sharper. Notably and most importantly, the FDM spectrum is fit by the form of Eq. 1.2, so the parameters of the peaks (such as the positions, widths and amplitudes) are known. At the same time, fitting $|I(\omega)|$ by Lorentzians would be a very challenging project. We also point out that the overall shape of the spectrum is reproduced well by the multi-scale FDM, while the single-scale version is very unstable for this signal because of the very big background.

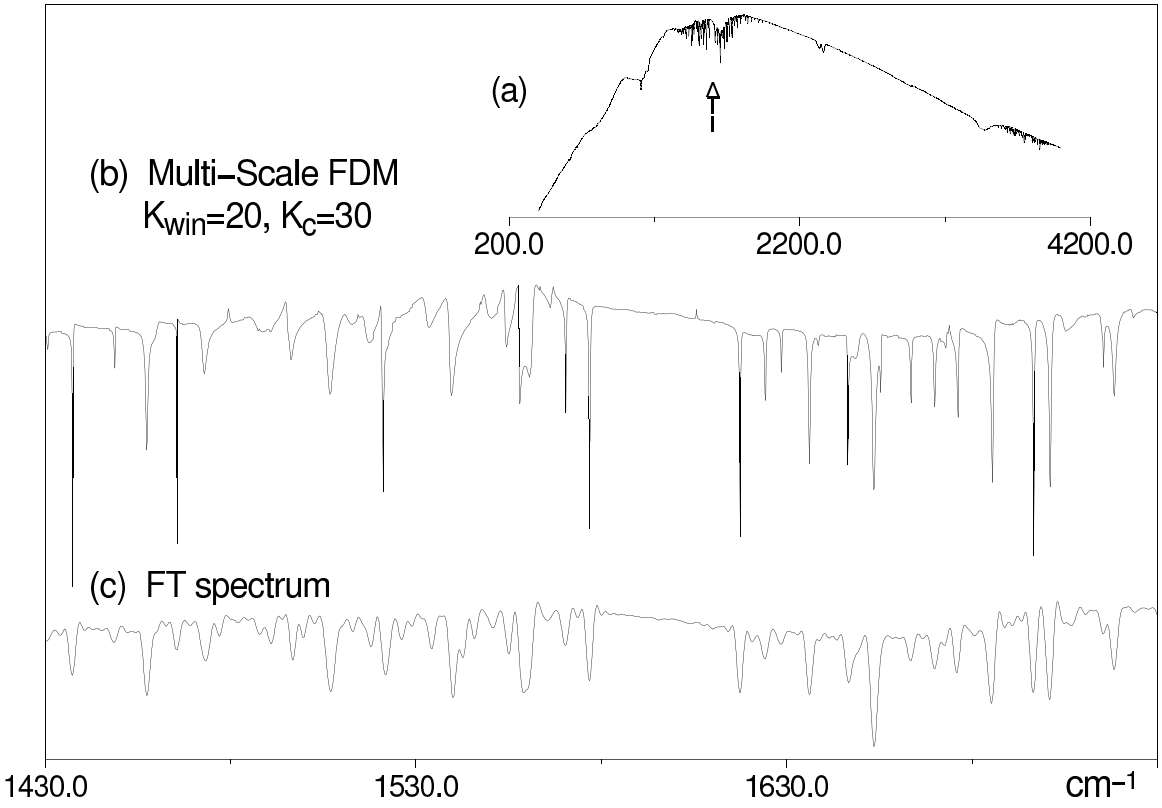

FIG. 5. *FT-IR spectrum (a) and an interesting part of the same spectrum processed by the multi-scale FDM with* $K_{\rm win} + K_c = 20 + 30 = 50$ *(b) and by FT (c). The interferogram contained 4744 data points.*

2.4 Extension to a 2D case

Here we extend the multi-scale Fourier basis to the 2D FDM by generalizing the 1D expressions of Section 2.2 accordingly. The previous formalism of 2D FDM can be found in Chapter I. A higher than two-dimensional case does not encounter any particular difficulties and the corresponding expressions are analogous.

To introduce a 2D multi-scale Fourier basis we generalize Eq. 2.8,

$$|\Psi_j) = \sum_{n_1=0}^{M_{1j}-1} \sum_{n_2=0}^{M_{2j}-1} e^{i\vec{n}(\vec{\varphi}_j - \vec{\Omega})} |\Phi_0) \tag{2.18}$$

with $\vec{\varphi}_j \equiv (\varphi_{1j}, \varphi_{2j})$ and M_{lj} being a function of φ_{lj}, $l = 1, 2$. A simple and numerically efficient setup could correspond to having two direct-product 2D grids: $\{\vec{\varphi}_j \equiv (\varphi_{1j_1}, \varphi_{2j_2})\}$, $j_l = 1, ..., K_{l\text{win}}$, with total size $K_{\text{win}} = K_{1\text{win}} \times K_{2\text{win}}$, and $\left\{\vec{\varphi}_j^{(\text{c})} \equiv \left(\varphi_{1j_1}^{(\text{c})}, \varphi_{2j_2}^{(\text{c})}\right)\right\}$, $j_l = 1, ..., K_{l\text{c}}$, with total size $K_{\text{c}} = K_{1\text{c}} \times K_{2\text{c}}$. In each dimension two independent 1D grids of values $\{\varphi_{lj_l}\}$, $j_l = l, ..., K_{l\text{win}}$, and $\left\{\varphi_{lj_l}^{(\text{c})}\right\}$, $j_l = 1, ..., K_{l\text{c}}$ have to be implemented, corresponding to the narrow band and coarse Fourier bases with $M_j = M_{l\text{max}}$ and $M_j = M_{l\text{c}}$, respectively, $M_{l\text{c}}$ being generally much smaller than the maximum allowed order $M_{l\text{max}} = N_{l\text{max}}/2 - 1$ of the Krylov basis in the l-th dimension dictated by the signal length $N_{l\text{max}}$ in this dimension. This construction allows to easily extend the procedure developed for the 1D multi-scale FDM to the present case.

By expanding the eigenvectors in the basis $\{\Psi_j\}$,

$$|\Upsilon_{lk}) = \sum_j \left[\mathbf{B}_{lk}\right]_j |\Psi_j) \ , \tag{2.19}$$

we can convert the two operator eigenvalue problems,

$$\hat{U}_l|\Upsilon_{lk}) = u_{lk}|\Upsilon_{lk}) \ , \ l = 1,2 \ , \tag{2.20}$$

into the two matrix generalized eigenvalue problems,

$$\mathbf{U}_l\mathbf{B}_{lk} = u_{lk}\mathbf{U}_0\mathbf{B}_{lk} \ , \ l = 1,2 \ , \tag{2.21}$$

where $\mathbf{U}_l$, $l = 1,2$, are the shortcuts for the matrix representations of the evolution operators $\hat{U}_l = e^{-i\tau_l\hat{\Omega}_l}$ with the eigenvalues $u_{lk} = e^{-i\tau_l\omega_{lk}}$ and U_0, the overlap matrix. By solving these two generalized eigenvalue problems one obtains the frequencies ω_{lk}; the associated eigenvectors $\mathbf{B}_{lk}$ yield b_{lk_l} and $T_{k_1k_2}$ needed to compute the amplitudes $d_{k_1k_2}$ by Eq. 1.39,

$$T_{k_1k_2} = \mathbf{B}_{1k_1}^T\mathbf{U}^{(0)}\mathbf{B}_{2k_2} \ , \tag{2.22}$$

$$b_{lk} = \sum_{\vec{\varphi}_j}[\mathbf{B}_{lk}]_j \sum_{n1=0}^{M_{1j}-1}\sum_{n2=0}^{M_{2j}-1} e^{-i\vec{n}\vec{\varphi}_j}c(\vec{n}) \ . \tag{2.23}$$

Finally, numerical expressions for the matrix elements of $\mathbf{U}_1$, $\mathbf{U}_2$ and $\mathbf{U}_0$ are obtained by using the 1D result of Eq. 2.11. Most generally, for any time vector $\vec{p} \equiv (\tau_1 p_1, \tau_2 p_2)$ the matrix elements of $\hat{U}^{(\vec{p})} \equiv e^{-ip_1\tau_1\hat{\Omega}_1}e^{-ip_2\tau_2\hat{\Omega}_2}$ are given by

$$\begin{aligned}\left[\mathbf{U}^{(\vec{p})}\right]_{jj'} &= \hat{S}_1\hat{S}_2 \sum_{\sigma_1=0,1} \frac{e^{i\sigma_1[M_{1j'}\tau_1(\varphi_{1j'}-\varphi_{1j})+\pi]}}{1-e^{i\tau_1(\varphi_{1j'}-\varphi_{1j})}} \\ &\times \sum_{\sigma_2=0,1} \frac{e^{i\sigma_2[M_{2j'}\tau_2(\varphi_{2j'}-\varphi_{2j})+\pi]}}{1-e^{i\tau_2(\varphi_{2j'}-\varphi_{2j})}} \\ &\times \sum_{n_1=\sigma_1 M_{1j'}}^{\sigma_1(M_{1j'}-1)+M_{1j}-1} \ \sum_{n_2=\sigma_2 M_{2j'}}^{\sigma_2(M_{2j'}-1)+M_{2j}-1} e^{i\vec{n}\vec{\varphi}_j}c(\vec{n}+\vec{p}) \ ,\end{aligned} \tag{2.24}$$

where $\hat{S}_l$ defines the symmetrization operator over the subscripts lj and lj' as in Eq. 1.24. When $\varphi_{lj} = \varphi_{lj'}$ Eq. 2.24 is rewritten according to Eq. 2.12. For example, for $\varphi_{1j} = \varphi_{1j'}$ we have

$$\begin{aligned}\left[\mathbf{U}^{(\vec{p})}\right]_{jj'} &= \hat{S}_2 \sum_{\sigma_2=0,1} \frac{e^{i\sigma_2[M_{2j'}\tau_2(\varphi_{2j'}-\varphi_{2j})+\pi]}}{1-e^{i\tau_2(\varphi_{2j'}-\varphi_{2j})}} \\ &\times \sum_{n_2=\sigma_2 M_{2j'}}^{\sigma_2(M_{2j'}-1)+M_{2j}-1} \ \sum_{n_1=0}^{2M_{1j}-2} e^{i\vec{n}\vec{\varphi}_j}c(\vec{n}+\vec{p}) \\ &\times (M_{1j} - |M_{1j} - n_1 - 1|) \ ,\end{aligned} \tag{2.25}$$

which can be trivially rewritten for the symmetric case of $\varphi_{2j} = \varphi_{2j'}$. For the case $\vec{\varphi}_j = \vec{\varphi}_{j'}$,

$$\left[\mathbf{U}^{(\vec{p})}\right]_{jj} = \sum_{n_1=0}^{2M_{1j}-2} \sum_{n_2=0}^{2M_{2j}-2} e^{i\vec{n}\vec{\varphi}_j} c(\vec{n}+\vec{p}) \times (M_{1j} - |M_{1j} - n_1 - 1|)(M_{2j} - |M_{2j} - n_2 - 1|) \; . \tag{2.26}$$

While the multi-scale basis works very well in 1D FDM, in 2D FDM, due to the problems described in Chapter I, applying multi-scale 2D FT basis should not be expected to be all-in-one solution. The preliminary results we obtained with 2D multi-scale FDM show that the *ersatz spectrum* obtained with single calculation still contains many artifacts, though sometimes it does show improvement compared to the case of single scale 2D FT basis. Therefore, we will still need to apply either *signal length averaging* or *pseudo-noise averaging* in order to obtain a clean and converged spectrum. But hopefully, with the multi-scale 2D FT basis, smaller spectral windows could be used so that less computational efforts will be needed to acquire similar results.

2.5 Conclusion and Remaining Problems

In this chapter, we demonstrated that the previous version of FDM may give an unstable solution under certain circumstances, when the Fourier spectral analysis can still provide quite meaningful spectra and is quite reliable. It was argued that the instability of FDM is caused by the use of a narrow band Fourier basis that is inadequate for representing very broad peaks in the presence of noise. Although there exist some primitive hybrid methods to obtain a reliable *ersatz spectrum*, it was proposed to improve the narrow band basis by including some coarse basis functions

to represent these broad features in low resolution. The use of such multi-scale Fourier basis leads to ersatz spectra that are no longer unstable but possess the high resolution quality of FDM. It provides a line list that accurately fits the spectrum by Lorentzians according to Eq. 1.31. Furthermore, with the coarse basis, one can use much smaller spectral windows for the local analysis which, in turn, reduces significantly the overall basis size per window and therefore the calculation time, as only very small matrices are to be diagonalized. In fact, the numerical bottleneck in the 1D multi-scale FDM is the construction of the U-matrices, generally requiring seconds on a small machine such as Pentium II 300 MHz PC. Since in 2D (and higher dimensional) FDM the total basis is the product of the 1D bases, the matrices to be diagonalized are generally large enough to make the diagonalization step the most time consuming, even with the multi-scale basis. Due to the cubic scaling of the eigenvalue solvers with respect to the matrix size, the significant basis reduction by using the multi-scale basis, will reduce enormously the computational cost of multi-dimensional FDM. At the present paper only the relevant equations for the 2D multi-scale FDM are given. The corresponding applications to the multi-dimensional signals will be tested in the near future.

While the multi-scale basis solves the instability problem in 1D FDM, in 2D FDM the instability problem is much worse. At present, we still need apply either signal length averaging or pseudo-noise averaging to get rid of artifacts. Precisely how the multi-scale basis helps to improve the performance of FDM is still not very clear. It is possible that multi-scale basis helps by improving the structure of matrices and making them less sigular. If this is true, other methods of removing the signularies like Signular Value Decomposition should be tried. In 2D FDM, the matrices usually have a bad structure with many signularities since the number of basis vectors are usually much more than number of the real peaks and the 2D signal is usually more noisy. Thus, the structures of the U matrices in 2D case need to be studied in details, and various methods of removing the signularies should be tried.

References

[1] D. Neuhauser, *J. Chem. Phys.* **93**, 2611-2616 (1990).

[2] M. R. Wall and D. Neuhauser, *J. Chem. Phys.* **102**, 8011-8022 (1995).

[3] V. A. Mandelshtam, and H. S. Taylor, *J. Chem. Phys.* **107**, 6756-6769 (1997).

[4] V. A. Mandelshtam, and H. S. Taylor, *J. Chem. Phys.* **108**, 9970-9977 (1998).

[5] V. A. Mandelshtam, H. S. Taylor, and A.J. Shaka, *J. Magn. Reson.* **133**, 304-312 (1998).

[6] V. A. Mandelshtam, H. Hu and A.J. Shaka, *Magn. Res. Chem.* **36**, S17-S28 (1998).

[7] H. Hu, Q.N. Van, V. A. Mandelshtam and A.J. Shaka, *J. Magn. Reson.* **134**, 76-87 (1998).

[8] J.W. Pang, T. Dieckmann, J. Feigon, D. Neuhauser, *J. Chem. Phys.* **108**, 8360-8368 (1998).

[9] M.R. Wall, T. Dieckmann, J. Feigon, D. Neuhauser, *Chem. Phys. Lett.* **291**, 465-470 (1998).

[10] V. A. Mandelshtam, Q.N. Van and A.J. Shaka, *J. Am. Chem. Soc.* **120**, 12161 (1998).

[11] V. A. Mandelshtam, N.D. Taylor, H. Hu, M. Smith, and A.J. Shaka, *Chem. Phys. Lett.* **305**, 209 (1999).

[12] H. Hu, A. A. De Angelis, V. A. Mandelshtam, A. J. Shaka *J. Magn. Reson.*, submitted

[13] V. A. Mandelshtam, *J. Chem. Phys.*, submitted

[14] G. Bodenhausen, R. Freeman, R. Niedermeyer, D. L. Turner, *J. Magn. Reson.* **26** 133 (1977)

[15] J. C. Hoch, A. S. Stern *NMR Data Processing*, (1996)

[16] D. J. States, R. A. Haberkorn, D. J. Ruben, *J. Magn. Reson.* **48** 286 (1982)

[17] C.B. Moler and G.W. Stewart, *J. Numer. Anal.* **10**, 241-256 (1973).

[18] V. A. Mandelshtam, and H. S. Taylor, *Phys. Rev. Lett.* **78**, 3274-3277 (1997).

[19] H. Barkhuijsen, R. de Beer, W. M. M. J. Bovée and *J. Magn. Reson.* **61**, 465-481 (1985).

[20] J. Tang and J. R. Norris,*J. Chem. Phys.* **84**, 5210-5211 (1986).

[21] H. Gesmar and J. J. Led, *J. Magn. Reson.* **76**, 183-192 (1988).

[22] G. Zhu and A. Bax, *J. Mang. Reson.* **90**, 405-410 (1990).

[23] J. Tang and J. Norris, *J. Magn. Reson.* **79**, 190-196 (1988)

[24] A. Bax, R. Freeman, and G. A. Morris, *J. Magn. Reson.* **43**, 333-338 (1981)

[25] R. Chen and H. Guo, *Chem. Phys. Lett.* **279**, 252-258 (1997)

[26] P. J. Hore, *J. Magn. Reson.* **55**, 283-300 (1983)

[27] G. A. Morris *J. Magn. Reson.* **91**, 547 (1991)

[28] V. A. Mandelshtam (unpublished)

[29] W.P. Aue, J. Karhan, and R.R. Ernst, *J. Chem. Phys.* **64**, 4226-4227 (1976).